

INTRIGUING PROPERTIES OF GENERATIVE CLASSIFIERS

Priyank Jaini*
Google DeepMind

Kevin Clark
Google DeepMind

Robert Geirhos*
Google DeepMind

ABSTRACT

What is the best paradigm to recognize objects—discriminative inference (fast but potentially prone to shortcut learning) or using a generative model (slow but potentially more robust)? We build on recent advances in generative modeling that turn text-to-image models into classifiers. This allows us to study their behavior and to compare them against discriminative models and human psychophysical data. We report four intriguing emergent properties of generative classifiers: they show a record-breaking human-like shape bias (99% for Imagen), near human-level out-of-distribution accuracy, state-of-the-art alignment with human classification errors, and they understand certain perceptual illusions. Our results indicate that while the current dominant paradigm for modeling human object recognition is discriminative inference, zero-shot generative models approximate human object recognition data surprisingly well.

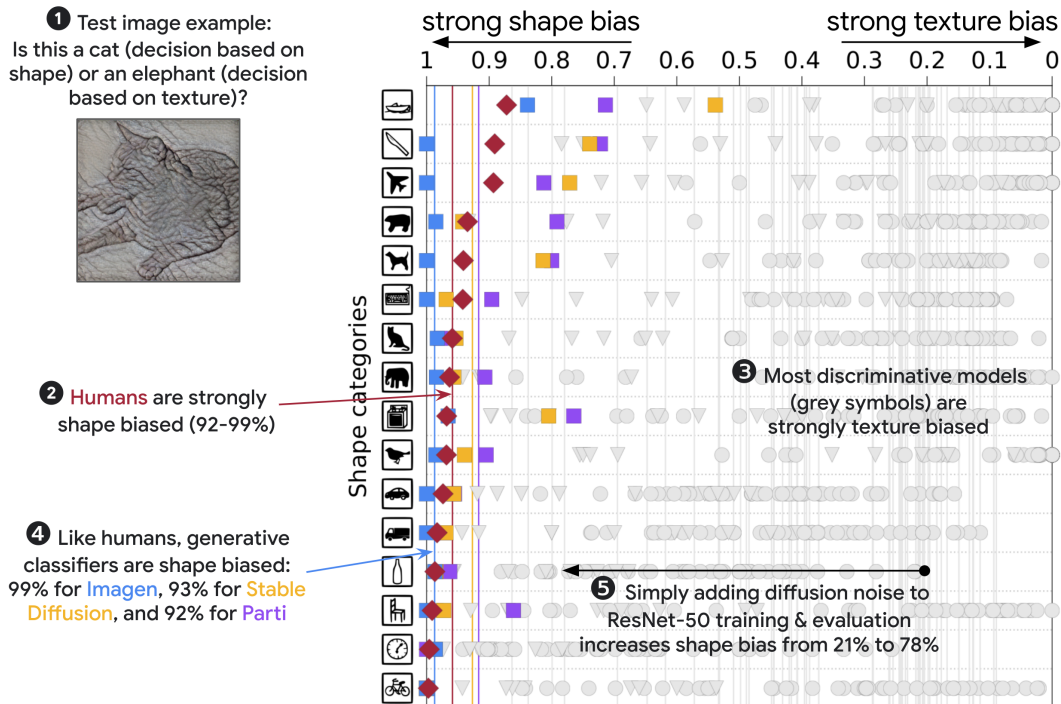


Figure 1: Zero-shot generative classifiers achieve a **human-level shape bias**: 99% for **Imagen**, 93% for **Stable Diffusion**, 92% for **Parti** and 92–99% for individual **human observers** (96% on average). Most discriminative models are texture biased instead.

*Equal contribution

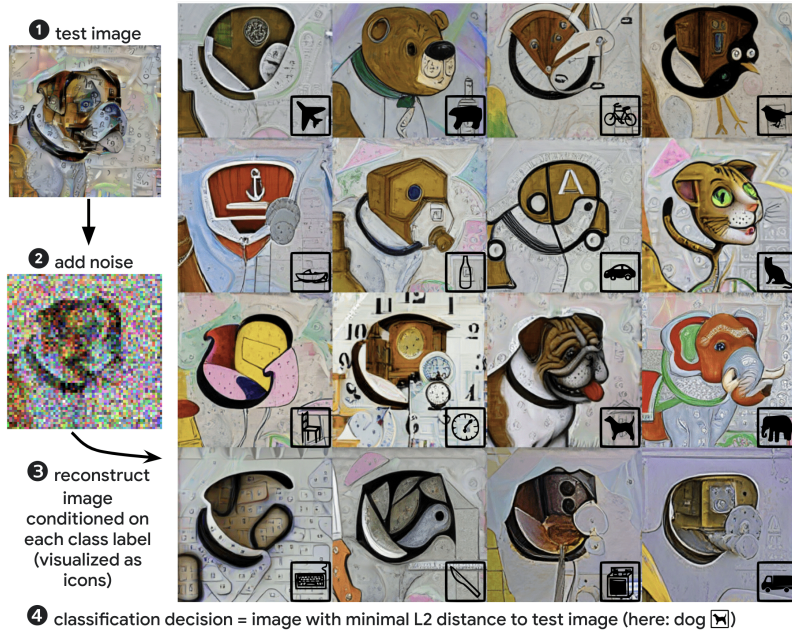


Figure 2: **Classification with a diffusion generative classifier.** Given a test image, such as a dog with clock texture (1), a text-to-image generative classifier adds random noise (2) and then reconstructs the image conditioned on the prompt “A bad photo of a <class>” (3). The reconstructed image closest to the test image in L_2 distance is taken as the classification decision; this estimates the diffusion variational lower bound (Clark & Jaini, 2023) (4). For visualization, class icons corresponding to the prompt class are superimposed on the bottom right of the reconstructed images.

1 INTRODUCTION

Many discriminative classifiers perform well on data similar to the training distribution, but struggle on out-of-distribution images. For instance, a cow may be correctly recognized when photographed in a typical grassy landscape, but is not correctly identified when photographed on a beach (Beery et al., 2018). In contrast to many *discriminatively* trained models, *generative* text-to-image models appear to have acquired a detailed understanding of objects: they have no trouble generating cows on beaches or dog houses made of sushi (Saharia et al., 2022). This raises the question: If we could somehow get classification decisions out of a generative model, how well would it perform out-of-distribution? For instance, would it be biased towards textures like most discriminative models or towards shapes like humans (Baker et al., 2018; Geirhos et al., 2019; Wichmann & Geirhos, 2023)?

We here investigate perceptual properties of *generative classifiers*, i.e., models trained to generate images from which we extract zero-shot classification decisions. We focus on two of the most successful types of text-to-image generative models—diffusion models and autoregressive models—and compare them to both discriminative models (e.g., ConvNets, vision transformers, CLIP) and human psychophysical data. Specifically, we focus on the task of visual object recognition (also known as classification) of challenging out-of-distribution datasets and visual illusions.

On a broader level, the question of whether perceptual processes such as object recognition are best implemented through a discriminative or a generative model has been discussed in various research communities for a long time. Discriminative inference is typically described as fast yet potentially prone to shortcut learning (Geirhos et al., 2020a), while generative modeling is often described as slow yet potentially more capable of robust inference (DiCarlo et al., 2021). The human brain appears to combine the best of both worlds, achieving fast inference but also robust generalization. How this is achieved, i.e. how discriminative and generative processes may be integrated has been described as “the deep mystery in vision” (Kriegeskorte, 2015, p. 435) and seen widespread interest in Cognitive Science and Neuroscience (see DiCarlo et al., 2021, for an overview). This mystery dates back to the idea of vision as inverse inference proposed more than 150 years ago

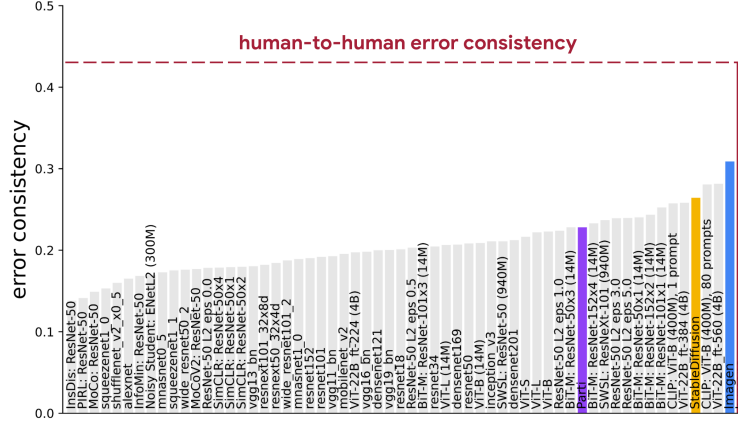


Figure 4: **Error consistency** across 17 challenging datasets (Geirhos et al., 2021). This metric measures whether errors made by models align with errors made by humans (higher is better).

on text prompts rather than class labels, we modify each label, y_k , to a text prompt using the template $y_k \rightarrow \text{A bad photo of a } y_k$. to generate classification decisions. Conceptually, our approach to obtain classification decisions is visualized in Figure 2.

Following Clark & Jaini (2023), we generate classification decisions from diffusion models like Stable Diffusion and Imagen by approximating the conditional log-likelihood $\log p_\theta(\mathbf{x}|y = y_k)$ using the diffusion variational lower bound (see Appendix A for a background on diffusion models):

$$\tilde{y} = \arg \max_{y_k} \log p_\theta(\mathbf{x}|y = y_k) \approx \arg \min_{y_k} \mathbb{E}_{\epsilon, t} [\|\mathbf{w}_t\| \mathbf{x} - \tilde{\mathbf{x}}_\theta(\mathbf{x}_t, y_k, t)\|^2] \quad (2)$$

For SD, \mathbf{x} is a latent representations whereas for Imagen \mathbf{x} consists of raw image pixels.

Evaluating $p_\theta(\mathbf{x}|y = y_k)$ for Parti amounts to performing one forward pass of the model since it is an autoregressive model that provides an exact conditional likelihood. Thus, for each of these models we evaluate the conditional likelihood, $p_\theta(\mathbf{x}|y = y_k)$, for each class $y_k \in [y_K]$ and assign the class with the highest likelihood obtained via Equation (1).

Model-vs-human datasets: We study the performance of these generative classifiers on 17 challenging out-of-distribution (OOD) datasets proposed in the model-vs-human toolbox (Geirhos et al., 2021). Of these 17 datasets, five correspond to a non-parametric single manipulation (sketches, edge-filtered images, silhouettes, images with a texture-shape cue conflict, and stylized images where the original image texture is replaced by the style of a painting). The other twelve datasets consist of parametric image distortions like low-pass filtered images, additive uniform noise, etc. These datasets are designed to test OOD generalization for diverse models in comparison to human object recognition performance. The human data consists of 90 human observers with a total of 85,120 trials collected in a dedicated psychophysical laboratory on a carefully calibrated screen (see Geirhos et al., 2021, for details). This allows us to compare classification data for zero-shot generative models, discriminative models and human observers in a comprehensive, unified setting.

Preprocessing: We preprocess the 17 datasets in the model-vs-human toolbox by resizing the images to 64×64 resolution for Imagen, 256×256 for Parti, and 512×512 for SD. We use the prompt, A bad photo of a y_k , for each dataset and every model. Although Imagen (Saharia et al., 2022) is a cascaded diffusion model consisting of a 64×64 low-resolution model and two super-resolution models, we only use the 64×64 base model for our experiments here. We use v1.4 of SD (Rombach et al., 2022) for our experiments that uses a pre-trained text encoder from CLIP to encode text and a pre-trained VAE to map images to a latent space. Finally, we use the Parti-3B model (Yu et al., 2022) consisting of an image tokenizer and an encoder-decoder transformer model that converts text-to-image generation to a sequence-to-sequence modeling problem.

Baseline models for comparison: As baseline discriminative classifiers, we compare Imagen, SD, and Parti against 52 diverse models from the model-vs-human toolbox (Geirhos et al., 2021) that are

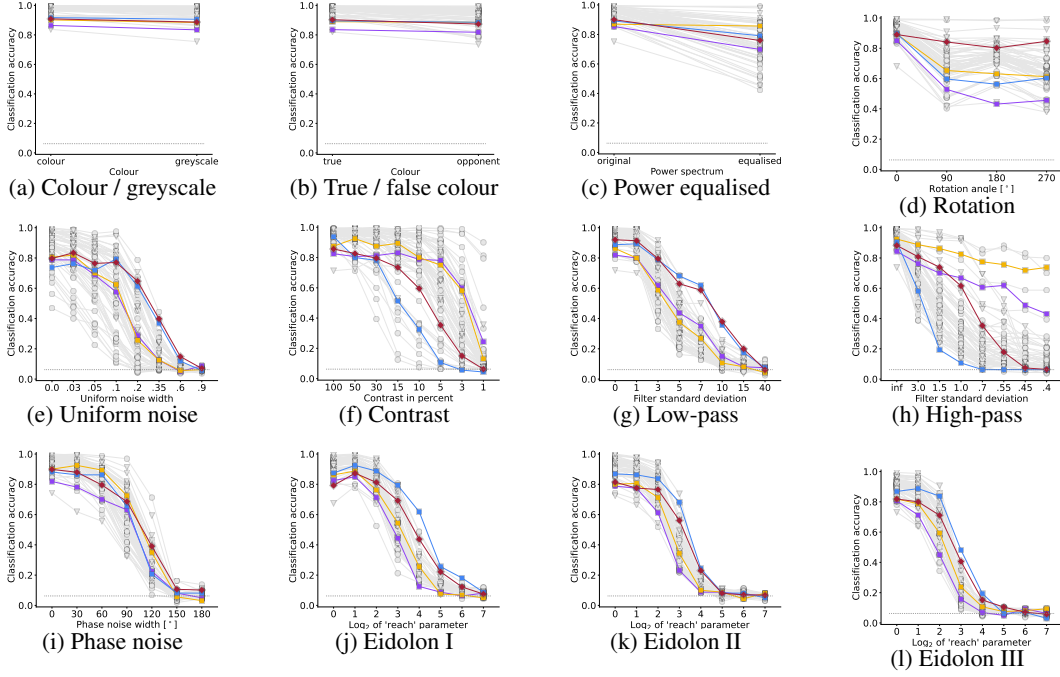


Figure 5: **Detailed out-of-distribution accuracy** for **Imagen**, **Stable Diffusion** and **Parti** in comparison to **human observers**. While not always aligning perfectly with human accuracy, the overall robustness achieved by both models is comparable to that of human observers even though these models are zero-shot, i.e. neither designed nor trained to do classification.

either trained or fine-tuned on ImageNet, three ViT-22B variants (Dehghani et al., 2023) (very large 22B parameter vision transformers) and CLIP (Radford et al., 2021) as a zero-shot classifier baseline. The CLIP model is based on the largest version, ViT-L/14@224px, and consist of vision and text transformers trained with contrastive learning. We use the CLIP model that uses an ensemble of 80 different prompts for classification (Radford et al., 2021). We plot all baseline discriminative models in grey and human subject data in red.

Metrics: We compare all the models over the 17 OOD datasets based on three metrics: (a) shape bias, (b) OOD accuracy and, (c) error consistency. Shape bias is defined by Geirhos et al. (2019) as the fraction of decisions that are identical to the shape label of an image divided by the fraction of decisions for which the model output was identical to either the shape or the texture label on a dataset with texture-shape cue conflict. OOD accuracy is defined as the fraction of correct decisions for a dataset that is not from the training distribution. Error consistency (see Geirhos et al., 2020b, for details) is measured in Cohen’s kappa (Cohen, 1960) and indicates whether two decision makers (e.g., a model and a human observer) systematically make errors on the same images. If that is the case, it may be an indication of deeper underlying similarities in terms of how they process images and recognize objects. Error consistency between models f_1 and f_2 is defined over a dataset on which both models are evaluated on exactly the same images and output a label prediction; the metric indicates the fraction of images on which $\mathbb{1}_{f_1(x)=y_x}$ is identical to $\mathbb{1}_{f_2(x)=y_x}$ (i.e., both models are either correct or wrong on the same image) when corrected for chance agreement. This ensures that an error consistency value of 0 corresponds to chance agreement, positive values indicate beyond-chance agreement (up to 1.0) and negative values indicate systematic disagreement (down to -1.0).

3 RESULTS: FOUR INTRIGUING PROPERTIES OF GENERATIVE CLASSIFIERS

3.1 HUMAN-LIKE SHAPE BIAS

Introduced by Geirhos et al. (2019), the *shape bias* of a model indicates to which degree the model’s decisions are based on object shape, as opposed to object texture. We study this phenomenon using the cue-conflict dataset which consists of images with shape-texture cue conflict. As shown in

model	model type	shape bias	OOD accuracy	error consist.
Imagen	zero-shot	99%	0.71	0.31
StableDiffusion	zero-shot	93%	0.69	0.26
Parti	zero-shot	92%	0.58	0.23
CLIP (80 prompts)	zero-shot	57%	0.71	0.28
ViT-22B-384 trained on 4B images	discriminative	87%	0.80	0.26
ViT-L trained on IN-21K	discriminative	42%	0.73	0.21
RN-50 trained on IN-1K	discriminative	21%	0.56	0.21
RN-50 trained w/ diffusion noise	discriminative	57%	0.57	0.24
RN-50 train+eval w/ diffusion noise	discriminative	78%	0.43	0.18

Table 1: **Benchmark results** for model-vs-human metrics (Geirhos et al., 2021). Within each model type (zero-shot vs. discriminative), the best result for each category is shown in bold.

Geirhos et al. (2021), most discriminative models are biased towards texture whereas humans are biased towards shape (96% shape bias on average; 92% to 99% for individual observers). Interestingly, we find that all three zero-shot generative classifiers show a shape bias that matches humans: Imagen achieves a stunning 99% shape bias, Stable Diffusion 93% and Parti a 92% shape bias.

As we show in Figure 1, Imagen closely matches or even exceeds human shape bias across nearly all categories, achieving a previously unseen shape bias of 99%. SD and Parti similarly achieve high shape bias (93 and 92% respectively). In Table 1, we report that all three generative classifiers significantly outperform ViT-22B (Dehghani et al., 2023), the previous state-of-the-art method in terms of shape bias, even though all three models are smaller in size, trained on less data, and unlike ViT-22B were not designed for classification.

3.2 NEAR HUMAN-LEVEL OOD ACCURACY

Humans excel at recognizing objects even if they are heavily distorted. *Do generative classifiers also possess similar out-of-distribution robustness?* We find that diffusion based models in Imagen and Stable Diffusion achieve an overall accuracy that is close to human-level robustness (cf. Figure 3) despite being zero-shot models. The detailed plots in Figure 5 show that on most datasets (except rotation and high-pass), the performance of all three generative classifiers approximately matches human responses. Additional results are in Table 3 and Figure 10 and 11 in the appendix.

Notably, all three models are considerably worse than humans in recognizing rotated images. Curiously, these models also struggle to generate rotated images when prompted with the text “A rotated image of a dog.” / “An upside – down image of a dog.” etc. This highlights an exciting possibility: evaluating generative models on downstream tasks like OOD datasets may be a quantitative way of gaining insights into the generation capabilities and limitations of these models.

On high-pass filtered images, Imagen performs much worse than humans whereas SD and Parti exhibit more robust performance. The difference in performance of Imagen and SD may be attributed to the weighting function used in Equation (2). Our choice of weighting function, $w_t := \exp(-7t)$, as used in Clark & Jaini (2023) tends to give higher weight to the lower noise levels and is thus bad at extracting decisions for high-frequency images. SD on the other hand operates in the latent space and thus the weighting function in Equation (2) effects its decisions differently than Imagen. Nevertheless, this indicates that even though Imagen and SD are diffusion-based models, they exhibit very different sensitivities to high spatial frequencies. Despite those two datasets where generative classifiers show varied performance, they overall achieve impressive zero-shot classification accuracy (near human-level performance as shown in Figure 3).

3.3 SOTA ERROR CONSISTENCY WITH HUMAN OBSERVERS

Humans and models may both achieve, say, 90% accuracy on a dataset but do they make errors on the same 10% of images, or on different images? This is measured by *error consistency* (Geirhos et al., 2020b). In Figure 4, we show the overall results for all models across the 17 datasets. While a substantial gap towards human-to-human error consistency remains, Imagen shows the most human-

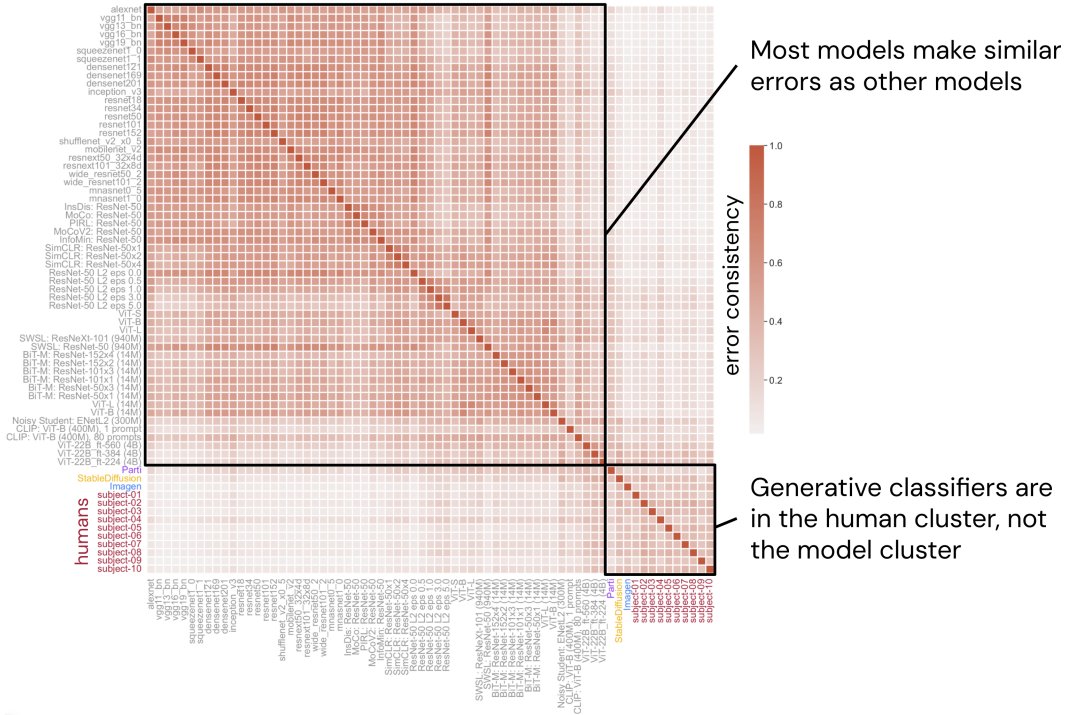


Figure 6: **Model-to-model error consistency** for ‘cue conflict’ images.

aligned error patterns, surpassing previous state-of-the-art (SOTA) set by ViT-22B, a large vision transformer (Dehghani et al., 2023). SD also exhibits error consistency closer to humans but lacks significantly compared to Imagen.

Additionally, a matrix plot of error consistency of all the models on cue-conflict images is shown in Figure 6. Interestingly, the plot shows a clear dichotomy between discriminative models that exhibit error patterns similar to each other, and generative models whose error patterns more closely match humans, thus they end up in the human cluster. While overall a substantial gap between the best models and human-to-human consistency remains (Figure 4), Imagen best captures human classification errors despite never being trained for classification. We report more detailed results in the appendix in Table 2 and Figures 10-17.

3.4 UNDERSTANDING CERTAIN VISUAL ILLUSIONS

Beyond quantitative benchmarking, we investigated a more qualitative aspect of generative models: whether they can understand certain visual illusions. In human perception, illusions often reveal aspects of our perceptual abilities that would otherwise go unnoticed. We therefore tested generative models on images that are visual illusions for humans. In contrast to discriminative models, generative classifiers offer a straightforward way to test illusions: for bistable images such as the famous rabbit-duck, we can prompt them to reconstruct based on ‘an image of a duck’ and ‘an image of a rabbit’. If they can (a) reconstruct images resembling the respective animal and (b) they place the reconstructed animal in the same location and pose as humans would, this can be seen as evidence that they “understand” the illusion. We find that this is indeed the case for generative models like Imagen, Stable Diffusion, and Muse (Chang et al., 2023). Since Parti cannot directly be used for image editing, we used Muse—a masking-based generative model that operates on VQ-VAE tokens similar to Parti—for this analysis instead of Parti; Muse on the other hand cannot be used as a classifier as explained in Appendix B. This ensures that our conclusions are not limited to diffusion models but cover generative models more broadly.

In Figure 7, we use four different images that are either bistable illusions for humans or images for which humans exhibit pareidolia (a tendency to see patterns in things, like a face in a rock). In

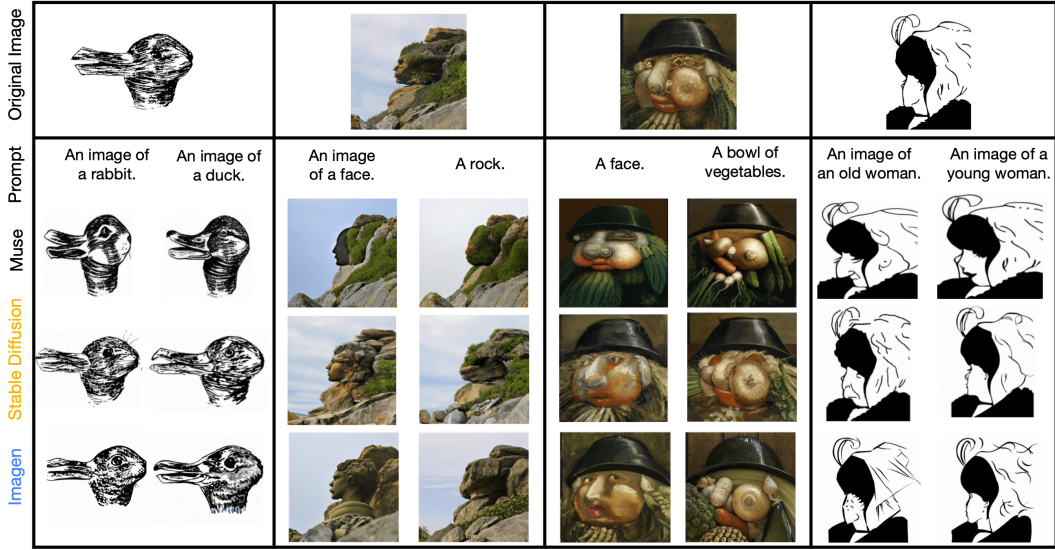


Figure 7: **Generative classifiers understand certain visual illusions** as indicated by their ability to reconstruct ambiguous images in a way that aligns with how humans perceive those images. For instance, they reconstruct a right-facing rabbit vs. a left-facing duck in the case of the bistable rabbit-duck illusion and place the face in the right location and pose for an image where humans show pareidolia (seeing patterns in things, like a face in a rock). Attribution for original images: App D.

all cases, the text-to-image generative models are able to recognize the illusion and recreate correct images conditioned on the respective text prompts. This indicates that these generative models share certain bistable illusions and pareidolia with human visual perception.

4 ANALYSIS: WHERE DOES THE INCREASED SHAPE BIAS ORIGINATE FROM?

In Section 3, we highlighted four *intriguing properties* of generative classifiers. The most striking emergent property amongst the four is the human-level shape bias demonstrated by these generative classifiers; a bias that no discriminative models so far was able to show. A natural question to ask is thus: *What aspect of these generative models causes such an increase in shape bias?*

We observed that for diffusion models like Imagen and Stable Diffusion, the recreated images used for classification were usually devoid of texture cues (for example see Figure 2). We posit that the denoising process used for classification (cf. Equation (2)) of the diffusion model might bias it towards capturing low-frequency information and thereby focuses on the global structure of the image as captured by the shape of an object. Indeed, in Figure 5, we observe that while generative classifiers are well within the range of other models for most datasets, they demonstrate very distinctive results on low-pass filtered images (also known as blurred); Imagen—the most shape-biased model—is on par with humans. Conversely, Imagen struggles to classify high-pass images. Could it be the case that these generative models put more emphasis on lower spatial frequencies whereas most textures are high frequency in nature?

If this is indeed the case, then performance on blurred images and shape bias should have a significant positive correlation. We tested this hypothesis empirically and indeed found a strong positive and highly significant correlation between the two (Pearson’s $r(58) = .59, p < 0.001$; Spearman’s $r(58) = .64, p < 0.001$). While this establishes a correlation between the two, it is not evidence for a causal link. We next hypothesized that the noise applied during diffusion training might encourage models to ignore high-frequency textures and focus on shapes. To test this prediction, we trained a standard ResNet-50 on ImageNet-1K (Russakovsky et al., 2015) by adding diffusion-style noise as a data augmentation during both training and evaluation. Interestingly, such a model trained with data augmented with diffusion style noise causes an increase in shape bias from 21% for a standard ResNet-50 to 78% as shown in Figures 1 and 13 and Table 1. This simple trick achieves a

substantially higher shape bias than the 62% observed by prior work when combining six different techniques and augmentations (Hermann et al., 2020).

This result shows that (i) diffusion style training biases the models to emphasize low spatial frequency information and (ii) models that put emphasis on lower spatial frequency noise exhibit increased shape bias. Other factors such as generative training, the quality and quantity of data, and the use of a powerful language model might also play a role. However, given the magnitude of the observed change in shape bias this indicates that diffusion-style training is indeed a crucial factor.

5 DISCUSSION

Motivation. While generative pre-training has been prevalent in natural language processing, in computer vision it is still common to pre-train models on labeled datasets such as ImageNet (Deng et al., 2009) or JFT (Sun et al., 2017). At the same time, generative text-to-image models like Stable Diffusion, Imagen, and Parti show powerful abilities to generate photo-realistic images from diverse text prompts. This suggests that these models learn useful representations of the visual world, but so far it has been unclear how their representations compare to discriminative models. Furthermore, discriminative models have similarly dominated computational modeling of human visual perception, even though the use of generative models by human brains has long been hypothesized and discussed. In this work, we performed an empirical investigation on out-of-distribution datasets to assess whether discriminative or generative models better fit human object recognition data.

Key results. We report four intriguing human-like properties of *generative* models: (1) Generative classifiers are the first models that achieve a human-like shape bias (92–99%); (2) they achieve near human-level OOD accuracy despite being zero-shot classifiers that were neither trained nor designed for classification; (3) one of them (Imagen) shows the most human-aligned error patterns that machine learning models have achieved to date; and (4) all investigated models qualitatively capture the ambiguities of images that are perceptual illusions for humans.

Implications for human perception. Our results establish generative classifiers as one of the leading behavioral models of human object recognition. While we certainly don’t resolve the “deep mystery of vision” (Kriegeskorte, 2015, p. 435) in terms of how brains might combine generative and discriminative models, our work paves the way for future studies that might combine the two. Quoting Luo (2022, p. 22) on diffusion, “It is unlikely that this is how we, as humans, naturally model and generate data; we do not seem to generate novel samples as random noise that we iteratively denoise.”—we fully agree, but diffusion may just be one of many implementational ways to arrive at a representation that allows for powerful generative modeling. Human brains are likely to use a different *implementation*, but they still may (or may not) end up with a similar *representation*.

Implications for machine perception. We provide evidence for the benefits of generative pre-training, particularly in terms of zero-shot performance on challenging out-of-distribution tasks. In line with recent work on using generative models for depth estimation (Zhao et al., 2023) or segmentation (Burgert et al., 2022; Brempong et al., 2022), this makes the case for generative pre-training as a compelling alternative to contrastive or discriminative training for vision tasks. Additionally, our experiments provide a framework to find potential bugs of generative models through classification tasks. For example, all the generative models performed poorly on the rotation dataset; those models also struggled to generate “rotated” or “upside-down” images of objects. Similar experiments can be used to evaluate generative models for undesirable behaviour, toxicity and bias.

Limitations. A limitation of the approach we used in the paper is the computational speed (as we also alluded to in Section 1). The approach does not yield a practical classifier. Secondly, all three models have different model sizes, input resolutions, and are trained on different datasets for different amounts of time, so the comparison is not perfect. Through including diverse generative models, our comparisons aim to highlight the strengths and weaknesses of generative models.

Future directions. Beyond the questions regarding how biological brains might combine generative and discriminative models, we believe it will be interesting to study how, and to what degree, language cross-attention influences the intriguing properties we find. Further, is denoising diffusion training a crucial component that explains the impressive performance of Imagen and SD? We hope our findings show generative classifiers as intriguing models for exploring exciting future directions.

ACKNOWLEDGMENTS

We would like to express our gratitude to the following colleagues (in alphabetical order) for helpful discussions and feedback: David Fleet, Katherine Hermann, Been Kim, Alex Ku, Jon Shlens, and Kevin Swersky.

REFERENCES

- Nicholas Baker, Hongjing Lu, Gennady Erlikhman, and Philip J Kellman. [Deep convolutional networks do not classify based on global object shape](#). *PLoS Computational Biology*, 14(12): e1006613, 2018.
- Sara Beery, Grant Van Horn, and Pietro Perona. [Recognition in terra incognita](#). In *Proceedings of the European Conference on Computer Vision*, pp. 456–473, 2018.
- Thomas G Bever and David Poeppel. [Analysis by synthesis: a \(re-\) emerging program of research for language and vision](#). *Biolinguistics*, 4(2-3):174–200, 2010.
- Emmanuel Asiedu Brempong, Simon Kornblith, Ting Chen, Niki Parmar, Matthias Minderer, and Mohammad Norouzi. [Denoising Pretraining for Semantic Segmentation](#). In *Proceedings of the IEEE/CVF Conference on Computer Vision and Pattern Recognition*, pp. 4175–4186, 2022.
- Ryan Burgert, Kanchana Ranasinghe, Xiang Li, and Michael S Ryoo. [Peekaboo: Text to Image Diffusion Models are Zero-Shot Segmentors](#). *arXiv preprint arXiv:2211.13224*, 2022.
- Huiwen Chang, Han Zhang, Jarred Barber, AJ Maschinot, Jose Lezama, Lu Jiang, Ming-Hsuan Yang, Kevin Murphy, William T Freeman, Michael Rubinstein, et al. [Muse: Text-To-Image Generation via Masked Generative Transformers](#). *arXiv preprint arXiv:2301.00704*, 2023.
- Kevin Clark and Priyank Jaini. [Text-to-image diffusion models are zero-shot classifiers](#). *arXiv preprint arXiv:2303.15233*, 2023.
- Jacob Cohen. [A coefficient of agreement for nominal scales](#). *Educational and Psychological Measurement*, 20(1):37–46, 1960.
- Peter Dayan, Geoffrey E Hinton, Radford M Neal, and Richard S Zemel. [The Helmholtz machine](#). *Neural Computation*, 7(5):889–904, 1995.
- Mostafa Dehghani, Josip Djolonga, Basil Mustafa, Piotr Padlewski, Jonathan Heek, Justin Gilmer, Andreas Peter Steiner, Mathilde Caron, Robert Geirhos, Ibrahim Alabdulmohsin, et al. [Scaling vision transformers to 22 billion parameters](#). In *International Conference on Machine Learning*, pp. 7480–7512. PMLR, 2023.
- Jia Deng, Wei Dong, Richard Socher, Li-Jia Li, Kai Li, and Li Fei-Fei. [Imagenet: A large-scale hierarchical image database](#). In *2009 IEEE conference on computer vision and pattern recognition*, pp. 248–255. Ieee, 2009.
- James J DiCarlo, Ralf Haefner, Leyla Isik, Talia Konkle, Nikolaus Kriegeskorte, Benjamin Peters, Nicole Rust, Kim Stachenfeld, Joshua B Tenenbaum, Doris Tsao, et al. [How does the brain combine generative models and direct discriminative computations in high-level vision?](#) 2021.
- Alexey Dosovitskiy, Lucas Beyer, Alexander Kolesnikov, Dirk Weissenborn, Xiaohua Zhai, Thomas Unterthiner, Mostafa Dehghani, Matthias Minderer, Georg Heigold, Sylvain Gelly, Jakob Uszkoreit, and Neil Houlsby. [An Image is Worth 16x16 Words: Transformers for Image Recognition at Scale](#). In *International Conference on Learning Representations*, 2021.
- Robert Geirhos, Patricia Rubisch, Claudio Michaelis, Matthias Bethge, Felix A. Wichmann, and Wieland Brendel. [ImageNet-trained CNNs are biased towards texture; increasing shape bias improves accuracy and robustness](#). In *International Conference on Learning Representations*, 2019.
- Robert Geirhos, Jörn-Henrik Jacobsen, Claudio Michaelis, Richard Zemel, Wieland Brendel, Matthias Bethge, and Felix A Wichmann. [Shortcut Learning in Deep Neural Networks](#). *Nature Machine Intelligence*, 2:665–673, 2020a.

- Robert Geirhos, Kristof Meding, and Felix A Wichmann. [Beyond accuracy: quantifying trial-by-trial behaviour of CNNs and humans by measuring error consistency](#). *Advances in Neural Information Processing Systems*, 33, 2020b.
- Robert Geirhos, Kantharaju Narayanappa, Benjamin Mitzkus, Tizian Thieringer, Matthias Bethge, Felix A Wichmann, and Wieland Brendel. [Partial success in closing the gap between human and machine vision](#). *Advances in Neural Information Processing Systems*, 34:23885–23899, 2021.
- Kaiming He, Xiangyu Zhang, Shaoqing Ren, and Jian Sun. [Delving deep into rectifiers: Surpassing human-level performance on ImageNet classification](#). In *Proceedings of the IEEE International Conference on Computer Vision*, pp. 1026–1034, 2015.
- Katherine Hermann, Ting Chen, and Simon Kornblith. The origins and prevalence of texture bias in convolutional neural networks. *Advances in Neural Information Processing Systems*, 33:19000–19015, 2020.
- Jonathan Ho, Ajay Jain, and Pieter Abbeel. [Denoising diffusion probabilistic models](#). *Advances in Neural Information Processing Systems*, 33:6840–6851, 2020.
- Diederik Kingma, Tim Salimans, Ben Poole, and Jonathan Ho. [Variational diffusion models](#). *Advances in Neural Information Processing Systems*, 34:21696–21707, 2021.
- Diederik P Kingma and Max Welling. [Auto-encoding Variational Bayes](#). *International Conference on Learning Representations*, 2014.
- Nikolaus Kriegeskorte. [Deep neural networks: a new framework for modeling biological vision and brain information processing](#). *Annual Review of Vision Science*, 1:417–446, 2015.
- Alex Krizhevsky, Ilya Sutskever, and Geoffrey E Hinton. [ImageNet classification with deep convolutional neural networks](#). In *Advances in Neural Information Processing Systems*, pp. 1097–1105, 2012.
- Calvin Luo. [Understanding diffusion models: A unified perspective](#). *arXiv preprint arXiv:2208.11970*, 2022.
- Andrew Ng and Michael Jordan. [On discriminative vs. generative classifiers: A comparison of logistic regression and naive Bayes](#). *Advances in Neural Information Processing Systems*, 14, 2001.
- Alec Radford, Jong Wook Kim, Chris Hallacy, Aditya Ramesh, Gabriel Goh, Sandhini Agarwal, Girish Sastry, Amanda Askell, Pamela Mishkin, Jack Clark, et al. [Learning transferable visual models from natural language supervision](#). In *International Conference on Machine Learning*, pp. 8748–8763. PMLR, 2021.
- Robin Rombach, Andreas Blattmann, Dominik Lorenz, Patrick Esser, and Björn Ommer. [High-resolution image synthesis with latent diffusion models](#). In *Proceedings of the IEEE/CVF Conference on Computer Vision and Pattern Recognition*, pp. 10684–10695, 2022.
- Olga Russakovsky, Jia Deng, Hao Su, Jonathan Krause, Sanjeev Satheesh, Sean Ma, Zhiheng Huang, Andrej Karpathy, Aditya Khosla, Michael Bernstein, Alexander C Berg, and Li Fei-Fei. [ImageNet Large Scale Visual Recognition Challenge](#). *International Journal of Computer Vision*, 115(3):211–252, 2015.
- Chitwan Saharia, William Chan, Saurabh Saxena, Lala Li, Jay Whang, Emily Denton, Seyed Kamyar Seyed Ghasemipour, Burcu Karagol Ayan, S Sara Mahdavi, Rapha Gontijo Lopes, et al. [Photorealistic Text-to-Image Diffusion Models with Deep Language Understanding](#). *Advances in Neural Information Processing Systems*, 2022.
- Lukas Schott, Jonas Rauber, Matthias Bethge, and Wieland Brendel. [Towards the first adversarially robust neural network model on MNIST](#). In *International Conference on Learning Representations*, 2018.

- Jascha Sohl-Dickstein, Eric Weiss, Niru Maheswaranathan, and Surya Ganguli. [Deep unsupervised learning using nonequilibrium thermodynamics](#). In *International Conference on Machine Learning*, pp. 2256–2265. PMLR, 2015.
- Yang Song and Stefano Ermon. [Improved techniques for training score-based generative models](#). *Advances in Neural Information Processing Systems*, 33:12438–12448, 2020.
- Yang Song, Jascha Sohl-Dickstein, Diederik P Kingma, Abhishek Kumar, Stefano Ermon, and Ben Poole. [Score-based generative modeling through stochastic differential equations](#). *arXiv preprint arXiv:2011.13456*, 2020.
- Chen Sun, Abhinav Shrivastava, Saurabh Singh, and Abhinav Gupta. [Revisiting unreasonable effectiveness of data in deep learning era](#). In *Proceedings of the IEEE international conference on computer vision*, pp. 843–852, 2017.
- Hermann von Helmholtz. *Handbuch der physiologischen Optik: mit 213 in den Text eingedruckten Holzschnitten und 11 Tafeln*, volume 9. Voss, 1867.
- Felix A Wichmann and Robert Geirhos. [Are Deep Neural Networks Adequate Behavioral Models of Human Visual Perception?](#) *Annual Review of Vision Science*, 9, 2023.
- Jiahui Yu, Yuanzhong Xu, Jing Yu Koh, Thang Luong, Gunjan Baid, Zirui Wang, Vijay Vasudevan, Alexander Ku, Yinfei Yang, Burcu Karagol Ayan, et al. [Scaling autoregressive models for content-rich text-to-image generation](#). *arXiv preprint arXiv:2206.10789*, 2(3):5, 2022.
- Alan Yuille and Daniel Kersten. [Vision as Bayesian inference: analysis by synthesis?](#) *Trends in Cognitive Sciences*, 10(7):301–308, 2006.
- Wenliang Zhao, Yongming Rao, Zuyan Liu, Benlin Liu, Jie Zhou, and Jiwen Lu. [Unleashing Text-to-Image Diffusion Models for Visual Perception](#). *arXiv preprint arXiv:2303.02153*, 2023.

Appendix

Table of Contents

A Background on diffusion models	13
B Muse as a classifier	14
C Limitations	14
D Image attribution	15
E Details on ResNet-50 training with diffusion noise	15
F Additional plots for model-vs-human benchmark	16
G Quantitative benchmark scores and rankings	16

A BACKGROUND ON DIFFUSION MODELS

Diffusion models (Sohl-Dickstein et al., 2015; Ho et al., 2020; Song et al., 2020; Song & Ermon, 2020) are latent variable generative models defined by a forward and reverse Markov chain. Given an unknown data distribution, $q(\mathbf{x}_0)$, over observations, $\mathbf{x}_0 \in \mathbb{R}^d$, the forward process corrupts the data into a sequence of noisy latent variables, $\mathbf{x}_{1:T} := \{\mathbf{x}_1, \mathbf{x}_2, \dots, \mathbf{x}_T\}$, by gradually adding Gaussian noise with a fixed schedule defined as:

$$q(\mathbf{x}_{1:T}|\mathbf{x}_0) := \prod_{t=1}^T q(\mathbf{x}_t|\mathbf{x}_{t-1}) \quad (3)$$

where $q(\mathbf{x}_t|\mathbf{x}_{t-1}) := \text{Normal}(\mathbf{x}_t; \sqrt{1-\beta_t}\mathbf{x}_{t-1}, \beta_t\mathbf{I})$. The reverse Markov process gradually denoises the latent variables to the data distribution with learned Gaussian transitions starting from $\text{Normal}(\mathbf{x}_T; 0, \mathbf{I})$ i.e.

$$p_{\theta}(\mathbf{x}_{0:T}) := p(\mathbf{x}_T) \cdot \prod_{t=0}^{T-1} p_{\theta}(\mathbf{x}_{t-1}|\mathbf{x}_t)$$

$p_{\theta}(\mathbf{x}_{t-1}|\mathbf{x}_t) := \text{Normal}(\mathbf{x}_{t-1}; \boldsymbol{\mu}_{\theta}(\mathbf{x}_t, t), \boldsymbol{\Sigma}_{\theta}(\mathbf{x}_t, t))$. The aim of training is for the forward process distribution $\{\mathbf{x}_t\}_{t=0}^T$ to match that of the reverse process $\{\tilde{\mathbf{x}}_t\}_{t=0}^T$ i.e., the generative model $p_{\theta}(\mathbf{x}_0)$ closely matches the data distribution $q(\mathbf{x}_0)$. Specifically, these models can be trained by optimizing the variational lower bound of the marginal likelihood (Ho et al., 2020; Kingma et al., 2021):

$$-\log p_{\theta}(\mathbf{x}_0) \leq -\text{VLB}(\mathbf{x}_0) := \mathcal{L}_{\text{Prior}} + \mathcal{L}_{\text{Recon}} + \mathcal{L}_{\text{Diffusion}}$$

$\mathcal{L}_{\text{Prior}}$ and $\mathcal{L}_{\text{Recon}}$ are the prior and reconstruction loss that can be estimated using standard techniques in the literature (Kingma & Welling, 2014). The (re-weighted) diffusion loss can be written as:

$$\mathcal{L}_{\text{Diffusion}} = \mathbb{E}_{\mathbf{x}_0, \varepsilon, t} \left[\|\mathbf{w}_t \|\mathbf{x}_0 - \tilde{\mathbf{x}}_{\theta}(\mathbf{x}_t, t)\|_2^2 \right]$$

with $\mathbf{x}_0 \sim q(\mathbf{x}_0)$, $\varepsilon \sim \text{Normal}(0, \mathbf{I})$, and $t \sim \mathcal{U}([0, T])$. Here, \mathbf{w}_t is a weight assigned to the timestep, and $\tilde{\mathbf{x}}_{\theta}(\mathbf{x}_t, t)$ is the model's prediction of the observation \mathbf{x}_0 from the noised observation \mathbf{x}_t . Diffusion models can be conditioned on additional inputs like class labels, text prompts, segmentation masks or low-resolution images, in which case $\tilde{\mathbf{x}}_{\theta}$ also takes a conditioning signal \mathbf{y} as input.

B MUSE AS A CLASSIFIER

In Figure 8, we visualize why we were not able to include Muse as a (successful) classifier in our experiments. Even on clean, undistorted images Muse achieved only approximately chance-level accuracy. This may, however, just be a limitation on how we attempted to extract classification decisions out of the model; it is very well possible that other approaches might work better.



Figure 8: **Muse as a classifier.** This figure illustrates why Muse reconstructions are often challenging to use for classification. Given a starting image of a bottle with bear texture, we here plot 16 reconstructions each prompted with a different label. The \mathcal{L}_2 distance to the original image is shown in red for all categories except the one with the lowest distance (here: top left), for which the distance is plotted in green. The images with the lowest distance (row 1 column 1: airplane; row 2 column 3: car, row 4 column 4: truck) appear to be categories for which the model is unable to generate a realistic reconstruction, and thus simply sticks close to the original image. The image generated by prompting with the correct shape category (bottle) is shown in row 2 column 2. Since Muse returns images fairly close to the original one if it is not able to generate a realistic reconstruction, the approach of measuring \mathcal{L}_2 distance between original and reconstruction is not a feasible classification approach for Muse.

C LIMITATIONS

As mentioned in the introduction, using a generative model comes with advantages and disadvantages: potentially better generalization currently comes at the cost of being slower computationally compared to standard discriminative models. While this doesn’t matter much for the purpose of analyses, it is a big drawback in practical applications and any approaches that improve speed would be most welcome—in particular, generating at least one prediction (i.e., image generation) per class as we currently do is both expensive and slow.

Furthermore, the models we investigate all differ from another in more than one ways. For instance, their training data, architecture, and training procedure is not identical, thus any differences between

the models cannot currently be attributed to a single factor. That said, through the inclusion of a set of diverse models covering pixel-based diffusion, latent space diffusion, and autoregressive models we seek to at least cover a variety of generative classifiers in order to ensure that the conclusions we draw are not limited to a narrow set of generative models.

D IMAGE ATTRIBUTION

Rabbit-duck image:

Attribution: Unknown source, Public domain, via Wikimedia Commons.

Link: <https://upload.wikimedia.org/wikipedia/commons/9/96/Duck-Rabbit.png>

Rock image:

Attribution: Mirabeau, CC BY-SA 3.0, via Wikimedia Commons.

Link: https://commons.wikimedia.org/wiki/File:Visage_dans_un_rocher.jpg

Vegetable portrait image:

Attribution: Giuseppe Arcimboldo, Public domain, via Wikimedia Commons.

Link: https://upload.wikimedia.org/wikipedia/commons/4/49/Arcimboldo_Vegetables.jpg

Woman image:

Attribution: W. E. Hill, Public domain, via Wikimedia Commons.

Link: https://upload.wikimedia.org/wikipedia/commons/5/5f/My_Wife_and_My_Mother-In-Law_%28Hill%29.svg

E DETAILS ON RESNET-50 TRAINING WITH DIFFUSION NOISE

We trained a ResNet-50 in exactly the same way as for standard, 90 epoch ImageNet training with the key difference that we added diffusion noise as described by the code below. Since this makes the training task substantially more challenging, we trained the model for 300 instead of 90 epochs. The learning rate was 0.1 with a cosine learning rate schedule, SGD momentum of 0.9, weight decay of 0.0001, and a per device batch size of 64. For diffusion style denoising we used a flag named “sqrt_alphas” which ensures that the noise applied doesn’t completely destroy the image information in most cases. We did not optimize any of those settings with respect to any of the observed findings (e.g., shape bias) since we were interested in generally applicable results.

Listing 1: Python example of how diffusion noise was added as a data augmentation technique.

```
# Copyright 2023 DeepMind Technologies Limited.  
#SPDX-License-Identifier: Apache-2.0
```

```
import dataclasses  
from typing import Sequence, Tuple  
import grain.tensorflow as tf_grain  
import jax  
import tensorflow as tf  
  
@dataclasses.dataclass(frozen=True)  
class AddNoise(tf_grain.MapTransform):  
    """Adds diffusion-style noise to the image."""  
    sqrt_alphas: bool = True  
  
    def map(self, features: FlatFeatures) -> FlatFeatures:  
        image = features["image"]  
        alpha = tf.random.uniform([])  
        if self.sqrt_alphas:  
            alpha = tf.sqrt(alpha)  
        std = tf.sqrt(1 - alpha * alpha)
```

```
image = image * alpha + std * tf.random.normal(image.shape)
features["image"] = image
features["noise_level"] = std
return features
```

F ADDITIONAL PLOTS FOR MODEL-VS-HUMAN BENCHMARK

We here plot detailed performance for all models with respect to a few different properties of interest / metrics:

- Aggregated performance across 17 datasets: Figure 9
- Out-of-distribution accuracy: Figure 10 for parametric datasets and Figure 11 for nonparametric datasets
- Model-to-human error consistency: Figure 10
- Human-to-human, model-to-model error consistency (for nonparametric datasets): Figures 6 and 14 to 17
- Shape bias: Figure 12 and Figure 13

All metrics are based on the model-vs-human toolbox and explained in more detail in (Geirhos et al., 2021).

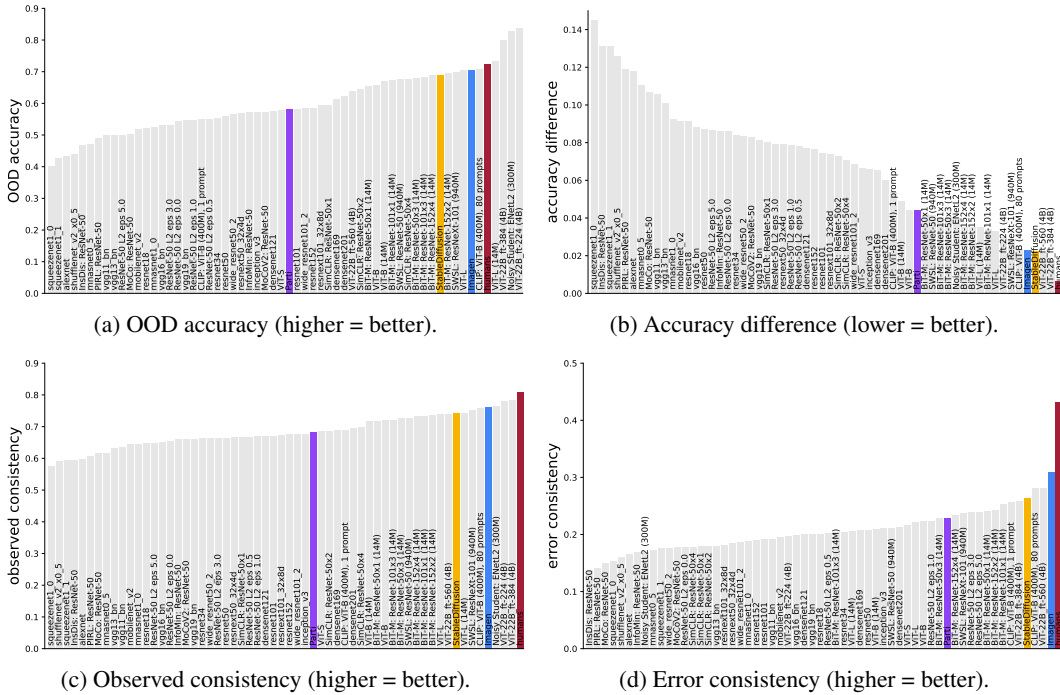


Figure 9: Benchmark results for different models, aggregated over datasets.

G QUANTITATIVE BENCHMARK SCORES AND RANKINGS

Table 2 and Table 3 list the detailed performance aggregated across 17 datasets for each model, with the former focusing on metrics related to “most human-like object recognition behavior” and the latter focusing on out-of-distribution accuracy.

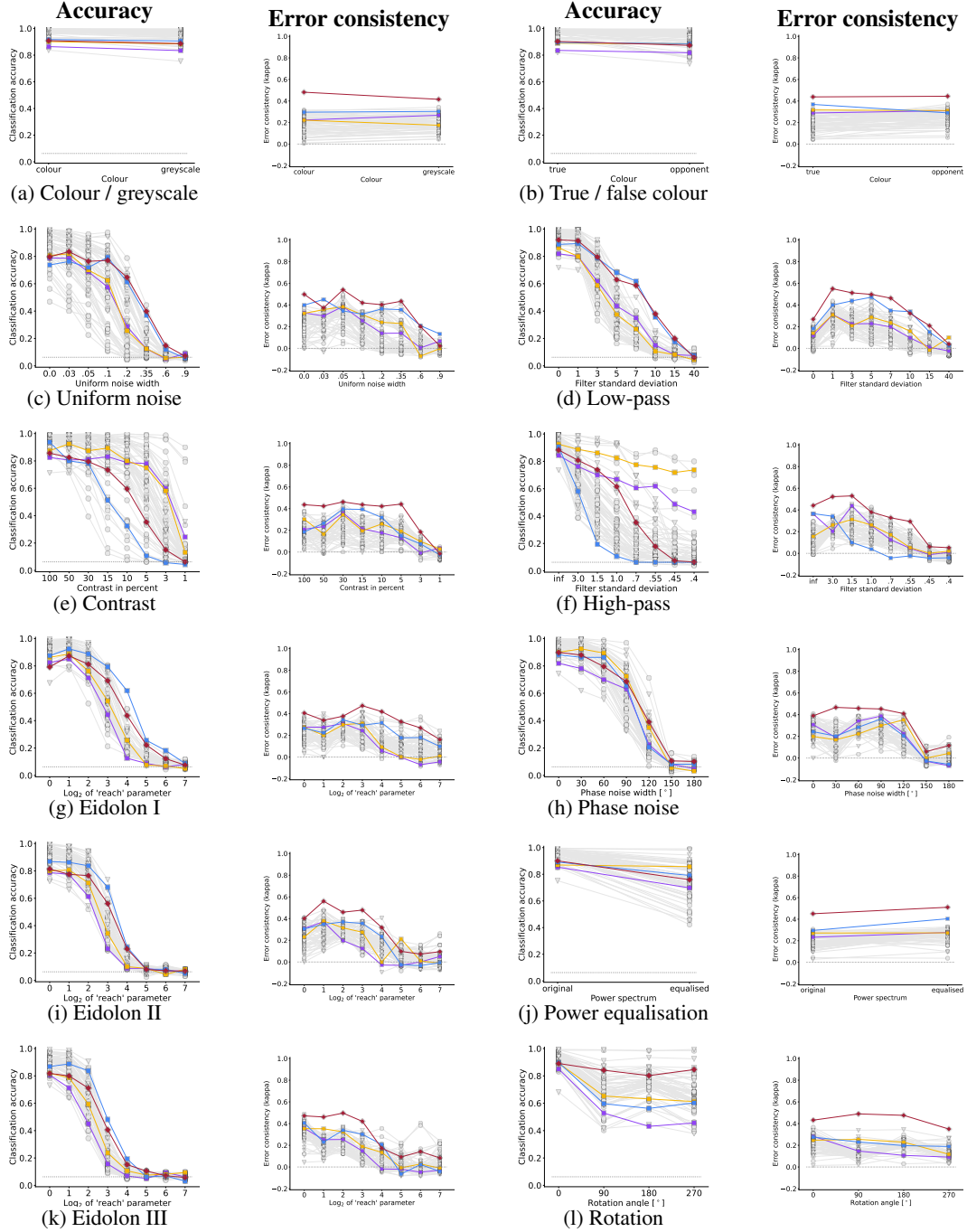


Figure 10: OOD accuracy and error consistency across all twelve parametric datasets from Geirhos et al. (2021). Error consistency results for nonparametric datasets are plotted in Figures 6 and 14 to 17.

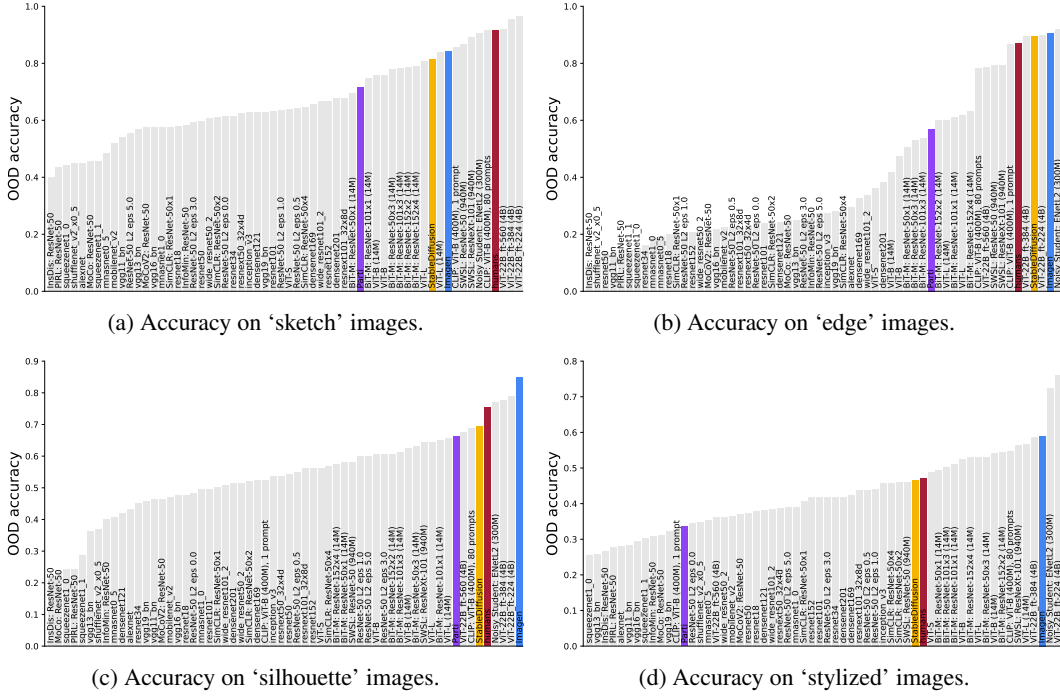


Figure 11: OOD accuracy on all four nonparametric datasets (i.e., datasets with only a single corruption type and strength).

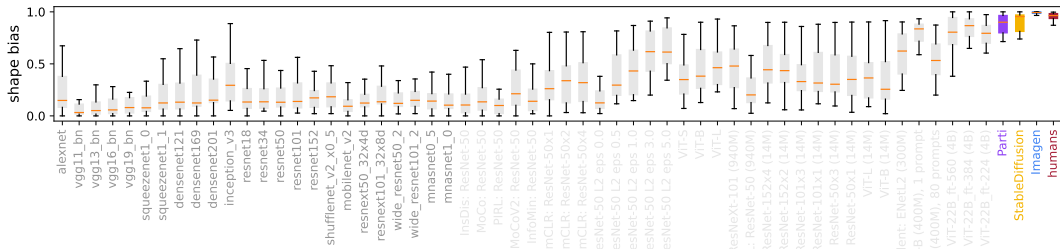


Figure 12: Zero-shot generative classifiers achieve a **human-level shape bias**: 99% for **Imagen**, 93% for **Stable Diffusion**, 92% for **Parti** and 92–99% for individual **human observers** (96% on average). This figure shows boxplots highlighting the spread across 16 categories for each model as a different way of visualizing the data from Figure 1.

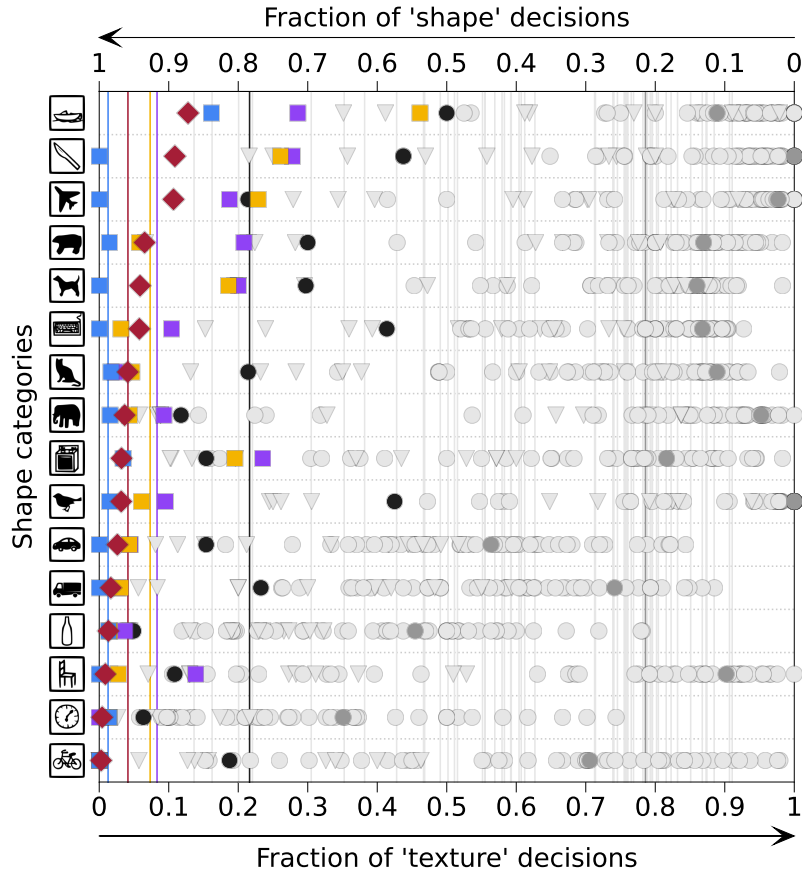


Figure 13: Shape bias before and after training with diffusion noise: This figure shows how ResNet-50 shape bias increases from 21% for a vanilla model (dark grey circles) to 78% when trained and evaluated with diffusion noise (black circles). Horizontal lines indicate the average shape bias across categories. Other models as in Figure 12.

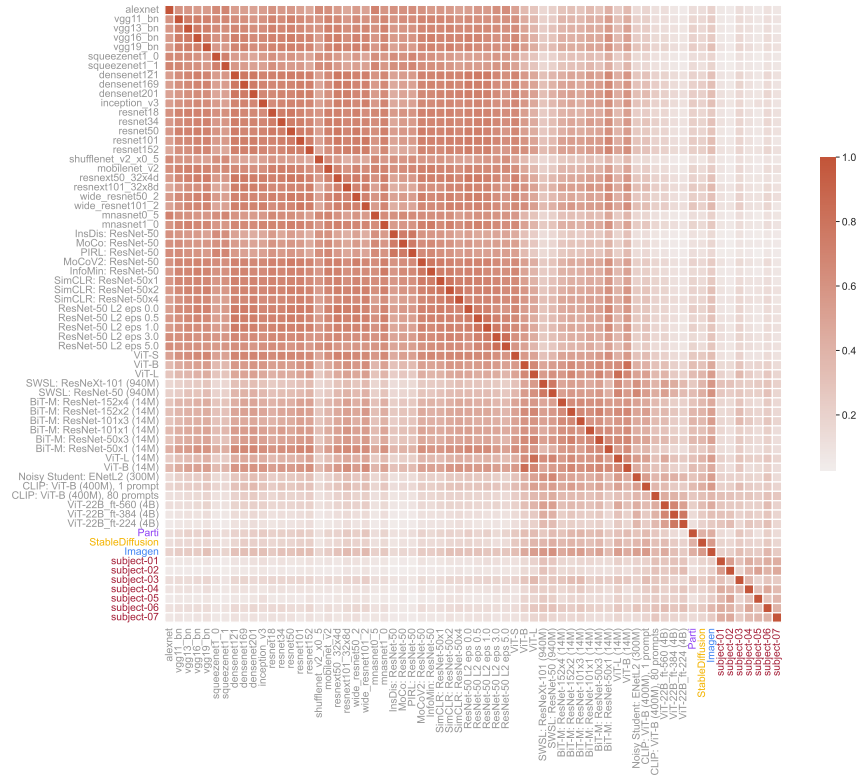


Figure 14: Error consistency for 'sketch' images.

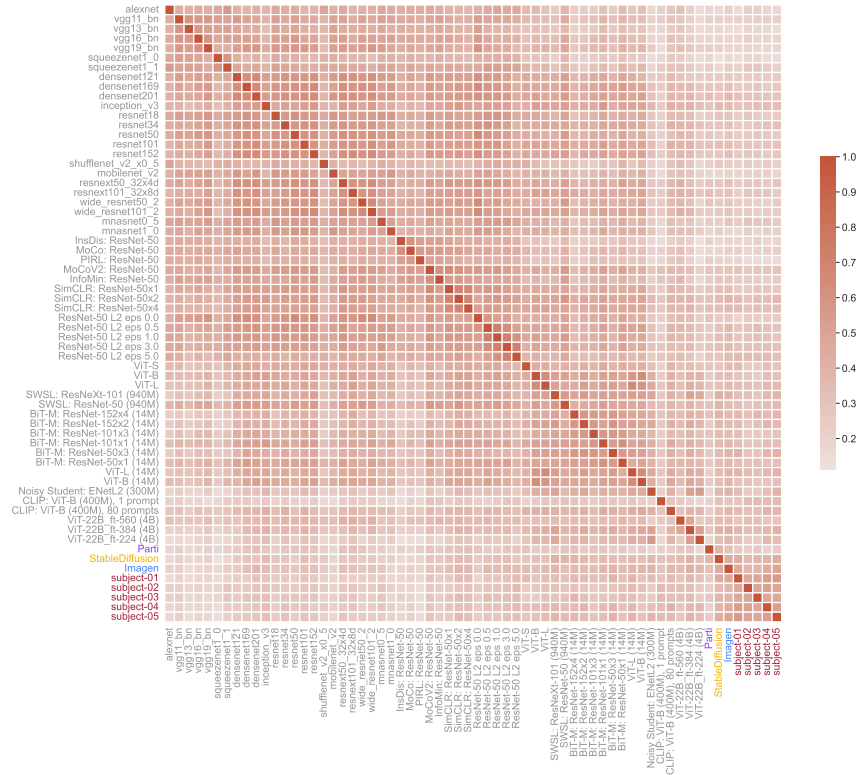


Figure 15: Error consistency for 'stylized' images.

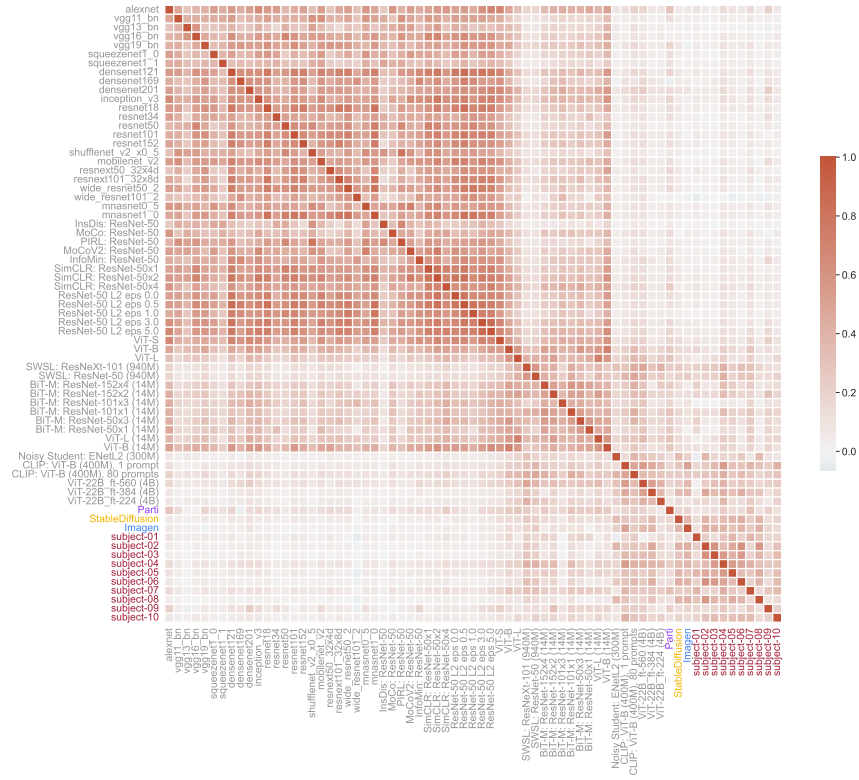


Figure 16: Error consistency for ‘edge’ images.

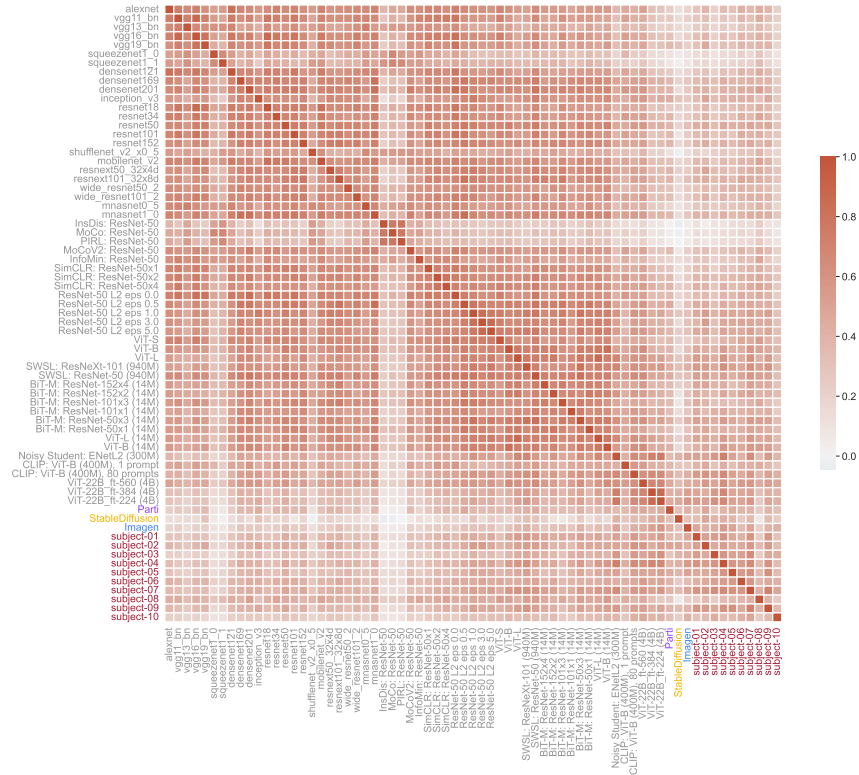


Figure 17: Error consistency for ‘silhouette’ images.

Table 2: Benchmark table of model results for most human-like behaviour, aggregated over all 17 datasets from Geirhos et al. (2021). The three metrics “accuracy difference” “observed consistency” and “error consistency” each produce a different model ranking. The mean rank of a model across those three metrics is used to rank the models on our benchmark.

model	accuracy diff. ↓	obs. consistency ↑	error consistency ↑	mean rank ↓
ViT-22B_ft-384 (4B)	0.018	0.783	0.258	2.333
Imagen (860M)	0.023	0.761	0.309	3.000
ViT-22B_ft-560 (4B)	0.022	0.739	0.281	4.333
CLIP: ViT-B (400M), 80 prompts	0.023	0.758	0.281	4.333
StableDiffusion	0.023	0.743	0.264	5.000
SWSL: ResNeXt-101 (940M)	0.028	0.752	0.237	8.000
BiT-M: ResNet-101x1 (14M)	0.034	0.733	0.252	9.333
BiT-M: ResNet-152x2 (14M)	0.035	0.737	0.243	10.000
ViT-L	0.033	0.738	0.222	11.667
BiT-M: ResNet-152x4 (14M)	0.035	0.732	0.233	12.667
ViT-L (14M)	0.035	0.744	0.206	14.000
ViT-22B_ft-224 (4B)	0.030	0.781	0.197	14.000
BiT-M: ResNet-50x3 (14M)	0.040	0.726	0.228	14.333
BiT-M: ResNet-50x1 (14M)	0.042	0.718	0.240	14.667
CLIP: ViT-B (400M), 1 prompt	0.054	0.688	0.257	16.000
SWSL: ResNet-50 (940M)	0.041	0.727	0.211	16.667
ViT-B	0.044	0.719	0.223	17.000
BiT-M: ResNet-101x3 (14M)	0.040	0.720	0.204	19.333
ViT-B (14M)	0.049	0.717	0.209	20.000
densenet201	0.060	0.695	0.212	20.333
Noisy Student: ENetL2 (300M)	0.040	0.764	0.169	22.333
ViT-S	0.066	0.684	0.216	22.333
densenet169	0.065	0.688	0.207	23.000
inception_v3	0.066	0.677	0.211	23.333
ResNet-50 L2 eps 1.0	0.079	0.669	0.224	26.667
ResNet-50 L2 eps 3.0	0.079	0.663	0.239	27.667
SimCLR: ResNet-50x4	0.071	0.698	0.179	30.333
wide_resnet101_2	0.068	0.676	0.187	30.333
ResNet-50 L2 eps 0.5	0.078	0.668	0.203	31.000
densenet121	0.077	0.671	0.200	31.000
SimCLR: ResNet-50x2	0.073	0.686	0.180	31.333
resnet152	0.077	0.675	0.190	31.667
resnet101	0.074	0.671	0.192	31.667
resnext101_32x8d	0.074	0.674	0.182	32.667
ResNet-50 L2 eps 5.0	0.087	0.649	0.240	32.667
resnet50	0.087	0.665	0.208	34.333
resnet34	0.084	0.662	0.205	35.000
vgg19_bn	0.081	0.660	0.200	35.667
resnext50_32x4d	0.079	0.666	0.184	36.333
SimCLR: ResNet-50x1	0.080	0.667	0.179	38.000
resnet18	0.091	0.648	0.201	40.333
vgg16_bn	0.088	0.651	0.198	40.333
wide_resnet50_2	0.084	0.663	0.176	41.667
MoCoV2: ResNet-50	0.083	0.660	0.177	42.000
mobilenet_v2	0.092	0.645	0.196	43.000
ResNet-50 L2 eps 0.0	0.086	0.654	0.178	43.333
mnasnet1_0	0.092	0.646	0.189	44.333
vgg11_bn	0.106	0.635	0.193	44.667
InfoMin: ResNet-50	0.086	0.659	0.168	45.333
vgg13_bn	0.101	0.631	0.180	47.000
mnasnet0_5	0.110	0.617	0.173	51.000
MoCo: ResNet-50	0.107	0.617	0.149	53.000
alexnet	0.118	0.597	0.165	53.333
squeezenet1_1	0.131	0.593	0.175	53.667
PIRL: ResNet-50	0.119	0.607	0.141	54.667
shufflenet_v2_x0.5	0.126	0.592	0.160	55.333
InsDis: ResNet-50	0.131	0.593	0.138	56.667
squeezenet1_0	0.145	0.574	0.153	57.000

Table 3: Benchmark table of model results for highest out-of-distribution robustness, aggregated over all 17 datasets from Geirhos et al. (2021).

model	OOD accuracy \uparrow	rank \downarrow
ViT-22B_ft-224 (4B)	0.837	1.000
Noisy Student: ENetL2 (300M)	0.829	2.000
ViT-22B_ft-384 (4B)	0.798	3.000
ViT-L (14M)	0.733	4.000
CLIP: ViT-B (400M), 80 prompts	0.708	5.000
Imagen (860M)	0.706	6.000
ViT-L	0.706	7.000
SWSL: ResNeXt-101 (940M)	0.698	8.000
BiT-M: ResNet-152x2 (14M)	0.694	9.000
StableDiffusion	0.689	10.000
BiT-M: ResNet-152x4 (14M)	0.688	11.000
BiT-M: ResNet-101x3 (14M)	0.682	12.000
BiT-M: ResNet-50x3 (14M)	0.679	13.000
SimCLR: ResNet-50x4	0.677	14.000
SWSL: ResNet-50 (940M)	0.677	15.000
BiT-M: ResNet-101x1 (14M)	0.672	16.000
ViT-B (14M)	0.669	17.000
ViT-B	0.658	18.000
BiT-M: ResNet-50x1 (14M)	0.654	19.000
SimCLR: ResNet-50x2	0.644	20.000
ViT-22B_ft-560 (4B)	0.639	21.000
densenet201	0.621	22.000
densenet169	0.613	23.000
SimCLR: ResNet-50x1	0.596	24.000
resnext101_32x8d	0.594	25.000
resnet152	0.584	26.000
wide_resnet101_2	0.583	27.000
resnet101	0.583	28.000
ViT-S	0.579	29.000
densenet121	0.576	30.000
MoCoV2: ResNet-50	0.571	31.000
inception_v3	0.571	32.000
InfoMin: ResNet-50	0.571	33.000
resnext50_32x4d	0.569	34.000
wide_resnet50_2	0.566	35.000
resnet50	0.559	36.000
resnet34	0.553	37.000
ResNet-50 L2 eps 0.5	0.551	38.000
CLIP: ViT-B (400M), 1 prompt	0.550	39.000
ResNet-50 L2 eps 1.0	0.547	40.000
vgg19_bn	0.546	41.000
ResNet-50 L2 eps 0.0	0.545	42.000
ResNet-50 L2 eps 3.0	0.530	43.000
vgg16_bn	0.530	44.000
mnasnet1_0	0.524	45.000
resnet18	0.521	46.000
mobilenet_v2	0.520	47.000
MoCo: ResNet-50	0.502	48.000
ResNet-50 L2 eps 5.0	0.501	49.000
vgg13_bn	0.499	50.000
vgg11_bn	0.498	51.000
PIRL: ResNet-50	0.489	52.000
mnasnet0.5	0.472	53.000
InsDis: ResNet-50	0.468	54.000
shufflenet_v2_x0.5	0.440	55.000
alexnet	0.434	56.000
squeezenet1_1	0.425	57.000
squeezenet1_0	0.401	58.000